Broadband cholesteric liquid crystal lens for chromatic aberration correction in catadioptric virtual reality optics

YANNANQI LI,[1,3] TAO ZHAN,[1,3] ZHIYONG YANG,[1] CHI XU,[1] PATRICK L. LIKAMWA,[1] KUN LI,[2] AND SHIN-TSON WU[1,*]

[1]*College of Optics and Photonics, University of Central Florida, Orlando, FL 32816, USA*
[2]*Goertek Electronics, 5451 Great America Parkway, Suite 301, Santa Clara, CA 95054, USA*
[3]*These authors contributed equally to this work*
[*]*swu@creol.ucf.edu*

Abstract: A planar and broadband cholesteric liquid crystal (CLC) lens is designed, fabricated, and hybridized with a refractive lens to form a catadioptric pancake lens for virtual reality (VR) displays. Due to their opposite optical dispersion behaviors, the chromatic aberration of the assembled pancake lens is dramatically suppressed, as verified by both ray-tracing analysis and experimental results. The demonstrated catadioptric pancake lens has great potential for next-generation VR displays.

1. Introduction

Recently, virtual reality (VR) displays have found widespread applications in gaming, healthcare, education, and engineering by offering a fully immersive environment. With an increasing demand for a more enjoyable visual experience, it is highly desirable for a VR headset to have high resolution, wide field-of-view (FOV), unnoticeable image blurs, compact size, and lightweight [1–3]. Nevertheless, full-color images presented in a large FOV could suffer from noticeable color breakups caused by the lateral chromatic aberration. For the chromatic aberration correction (CAC), both optical [4–8] and digital [9,10] compensation methods have been developed. Along with the concern of processing time and power consumption, digital CAC still cannot eliminate the chromatic aberrations caused by the spectral bandwidth of red, green, and blue (RGB) channels. On the other hand, optical CAC is promising and has been widely attempted in achromatic imaging systems.

   To fulfill CAC in VR systems, an intuitive way is to engage another refractive lens to form an achromat doublet lens. However, this approach makes the system bulkier and heavier. Zhan, et al. recently developed a new method for CAC by combining a broadband Pancharatnam-Berry (PB) phase lens with a refractive Fresnel singlet, making use of their opposite chromatic dispersions [11]. Since the diffractive lens is simply a polymer film, it does not increase the volume of VR systems. Compared to the optical configuration utilizing a transmissive light path in VR, catadioptric optics (i.e., pancake lens) is more promising and provides better optical performance with an appealing form-factor [12–15]. In the realm of folded optics, a singlet lens is still confronted with the chromatic aberration issue at the peripheral fields in a large FOV. To mitigate color breakups, here we propose a novel polarization-based pancake lens with the integration of a broadband cholesteric liquid crystal (CLC) lens. This type of diffractive and planar CLC lens was first demonstrated in [16]. Different from transmissive PB lenses [17–19], such a CLC lens can converge or diverge the reflected light with the same handedness, depending on the incident direction. To present full-color images in VR displays, the reflective spectrum of the CLC lens should be broadened to cover the RGB spectrum from ~450 nm to ~650 nm.

In this paper, we demonstrate a polarization-based pancake lens for catadioptric VR by applying a fabricated broadband CLC lens to correct the chromatic aberration. Exploiting the opposite chromatic dispersions, both ray-tracing analysis and experimental results prove that the lateral chromatic aberration can be suppressed significantly, especially at a large FOV. Such a broadband CLC lens is also promising for imaging and display systems, and our proposed novel pancake lens has potential applications in catadioptric VR display systems.

2. Working principle

2.1. Broadband CLC lens

Compared to traditional transmissive PB lenses, CLC lenses exhibit a shorter period along the direction perpendicular to the lens surface. Figure 1(a) illustrates the top view of the LC anisotropic axis distribution. In the longitudinal direction, it induces a vertical periodicity defined as the distance by which LC directors rotate 180°. The periodicity is equal to one-half of the cholesteric pitch length p_0. The established Bragg structure enables a reflective spectral bandwidth, which is determined by the LC birefringence (Δn) and pitch length as $\Delta \lambda = \Delta n p_0$. Several methods have been developed to broaden $\Delta \lambda$ by inducing a gradually changing period in the wave propagation direction [20–22]. Figure 1(b) depicts the cross-sectional view of the twisted and gradient structure in the z-direction. The shortest pitch is usually at the bottom of the cell and the longest one is on the top, originating from the movement of diacrylate molecule and resulting in an uneven distribution of chiral dopants [20]. The acquired phase (φ) through a CLC lens can be evaluated from the optical path difference between the lens center and edge as:

$$\varphi = \frac{2\pi}{\lambda}(\sqrt{r^2 + f^2} - f), \tag{1}$$

where λ is the wavelength used in the imaging system, r is the lens radius, and f is the focal length. When the lens radius is much smaller than the focal length ($r \ll f$), Eq. (1) can be approximated as $f \approx \pi r^2 / \lambda \varphi$. The CLC lens can reflect and converge or diverge the incident light with the same handedness, say right-handed circularly polarized (RCP) light, but transmits the opposite handedness (LCP). Detailed working principles of the CLC lens have been described in [23].
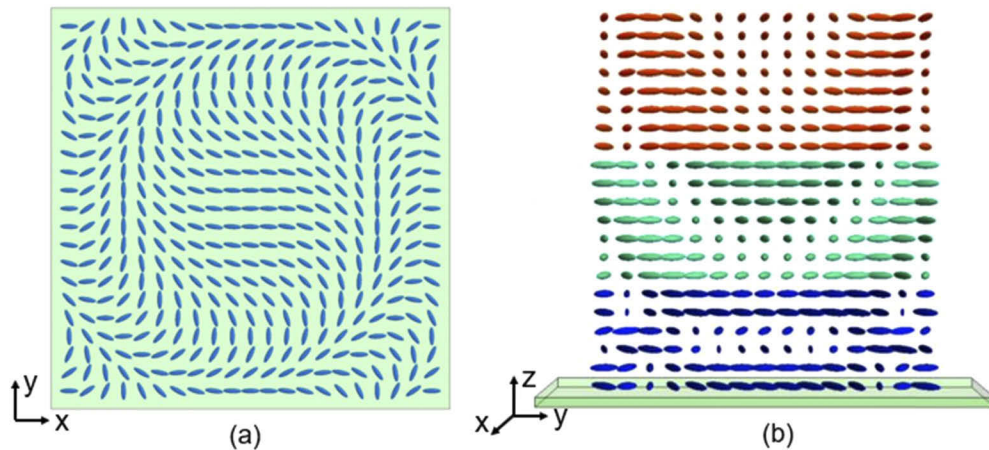

Fig. 1. (a) Top view of schematic LC director orientation in a CLC lens. (b) Cross-sectional view of the proposed broadband CLC lens with gradient pitches along the wave propagation direction.

2.2. Polarization-based pancake lens

The design for CAC should follow the principle similar to that of an achromatic doublet [24]:

$$\frac{K_{refractive}}{V_{refractive}} + \frac{K_{diffractive}}{V_{diffractive}} = 0, \tag{2}$$

where K and V are the corresponding optical power and Abbe number. For a refractive lens, the chromatic aberration can be characterized by V, which is defined as:

$$V_r = \frac{n_d - 1}{n_f - n_c}, \tag{3}$$

where n_c, n_d, and n_f are the refractive indices of the material at λ_c=656.3 nm, λ_d=589.3 nm, and λ_f=486.1 nm, respectively. In the visible spectral region, most of optical materials used in refractive lenses exhibit a decreasing refractive index as the wavelength increases, manifesting a positive V_r. Fortunately, opposite to refractive elements, diffractive optics have a negative dispersion characterized as [5]:

$$V_d = \frac{\lambda_d}{\lambda_f - \lambda_c}. \tag{4}$$

This opposite dispersive behavior originates from the wavelength dependence of the focal length in holographic lenses. No matter what kind of LC reactive mesogen materials are employed, the diffractive elements hybridized with refractive lenses can balance the chromatic aberration because of their intrinsic opposite dispersions. Figure 2 depicts the chromatic and achromatic performances of a single lens and a hybrid lens.
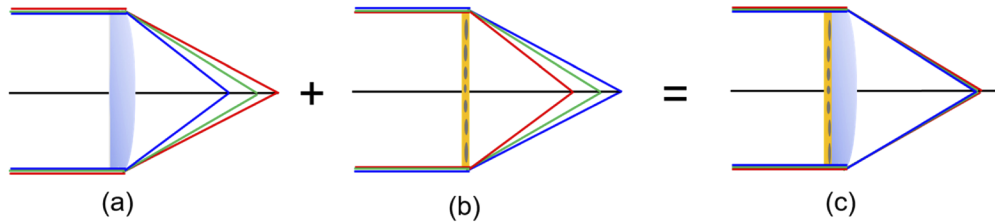

Fig. 2. (a) Chromatic aberration of a refractive lens. (b) Opposite chromatic aberration of a diffractive lens. (c) Achromatic performance of the hybrid lens.

A traditional polarization-based pancake lens [14] is usually composed of four parts: half-mirror, refractive lens, quarter-wave plate (QWP), and reflective polarizer, as illustrated in Fig. 3(a). The severity of chromatic aberration of this system is mainly determined by the refractive singlet. To suppress the chromatic aberration, we propose a novel structure consisting of a display panel and a set of optical components arranged in a pancake configuration, as Fig. 3(b) depicts. The CLC lens serves as a diffractive element for CAC, which also displaces the QWP and the reflective polarizer in the conventional systems. As shown in Fig. 3(b), the outgoing light from the liquid crystal display (LCD) panel passing through a broadband right-handed circular polarizer becomes RCP light. Next, it goes through the half-mirror and is reflected by the broadband CLC lens with the same handedness. Then the half-mirror reflects the RCP light and switches it to LCP, which can directly pass through the CLC lens after traveling through the cavity three times. A non-negligible factor is the light leakage shown in Fig. 3. For both designs, due to insufficient reflection efficiency of the reflective polarizer or the CLC lens, the leaked light would cause undesirable ghost images. An effective way to block the stray light is to place a broadband left-handed circular polarizer behind the CLC lens to absorb it.
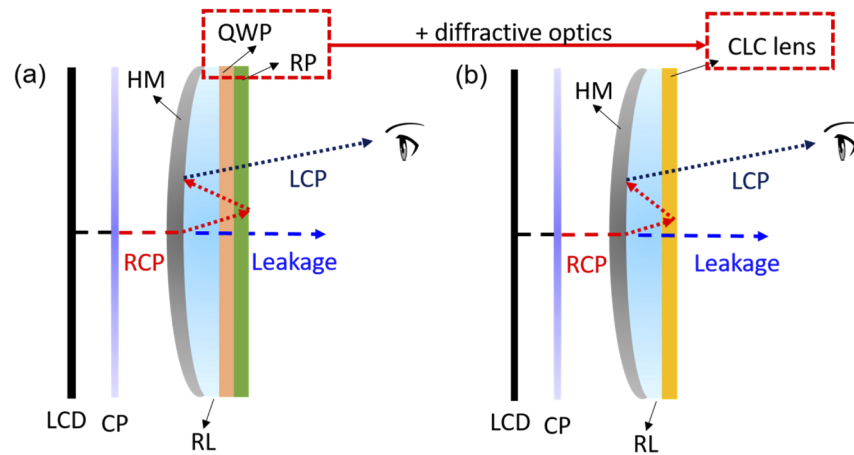
Fig. 3. System design of the polarization-based pancake lens for VR: (a) Traditional pancake lens, and (b) our proposed hybrid pancake lens. CP: circular polarizer; HM: half-mirror; RL: refractive lens; QWP: quarter-wave plate; RP: reflective polarizer.

3. Design and experiment

3.1. Pre-design

A commercial software OpticStudio is used to do the sequential raytracing and optimization to obtain a decent focal length of CLC lens for guiding the fabrication. Three wavelengths are set at Fraunhofer C, d, and F spectral lines (656.3 nm, 589.3 nm, and 486.1 nm), respectively. During simulations, the glass substrate thickness (about 1 mm) of the CLC lens is also taken into consideration to make the raytracing model closer to our practical prototype. The surface of hologram 1 in Zemax is applied for modeling the diffractive behavior of the CLC lens, and the medium behind the hologram is set as a mirror [25]. The construction wavelength is 457 nm, and the diffraction is the first order. It is noteworthy that OpticStudio only models the holograms to the extent of deviating ray paths. Therefore, the relative reflectance of the hologram, and the efficiency and light leakage of the system are not included in this simulation.

The plano-convex refractive lens employed in the system is purchased from Thorlabs. It is made of BK7 with f=124.6 mm and D=25.4 mm. The designed system has a 2 mm eyebox with a circular FOV of 100° accompanied by an eye relief of 7 mm. The optimized focal length of the CLC lens is 778 mm in virtue of operands by characterizing standard spot diagrams and lateral color shift. The simulation results will be discussed later.

3.2. Device fabrication

Unlike a polymeric film whose thickness is usually limited to 1~3 μm, to establish Bragg reflection, a thicker cell is required in order to achieve a broader reflection band, especially when we use a gradient pitch approach. Nevertheless, a thick cell may introduce CLC misalignment defects due to weaker anchoring energy in the bulk, resulting in a non-negligible scattering loss. To avoid such undesirable CLC misalignment, the cell gap (d) should be controlled under 8 μm according to our several experimental attempts.

For 2D patterning on substrates, a photo-alignment layer was spin-coated onto a cleaned glass substrate at 800 rpm for 5 s and then 3,000 rpm for 30 s to create a uniform thin film. In this work, brilliant yellow (BY) was used as the photo-alignment material, which was dissolved in dimethylformamide (DMF) solution with a concentration of 0.4% by weight. We used two glass substrates coated with BY to fabricate a cell with d~7 μm. Then the assembled cell was

exposed to the interference patterns generated by the polarization interferometry method [17]. The diameter of the exposed area is about 1 inch. After exposure, a CLC mixture was infiltrated into the cell at 110°C and then cooled down in the air to the room temperature (22°C). The CLC mixture consists of 90.13% LC host BL038 (Merck), 2.67% chiral dopant R5011 (HCCH, China), 3% diacrylate reactive mesogen RM257, 3% chiral-diacrylate SL04151, 0.2% photo-initiator Irg819, and 1% UV dye (Avobenzone, MakingCosmetics). The molecular structure of the UV dye is shown in Fig. 4. We measured the UV dye absorption at 390 nm using a linearly polarized light. The measured dichroic ratio of the UV dye is ~2:1. The dichroic characteristic in principle may induce a weak polarization state for the incident unpolarized UV light, which in turn affects the molecular orientation of brilliant yellow during the curing process. However, such a small influence can be ignored in our experiment because the gradient pitch is formed along the light propagation direction. The photo-initiator helps accelerate the chemical reaction. To maximize the intensity gradience from the entrance side to the exit side, we exposed the cell with a weak UV intensity ~0.1mW/cm^2 for 10 mins. With the help of photo-initiators, the diacrylates start to move and react, leading to an uneven distribution of chiral dopants, which in turn creates gradient pitch lengths for broadening the reflection band. Figure 4 shows the fabrication sequences. The focal length of the fabricated CLC lens is ~770 mm at λ=457 nm.
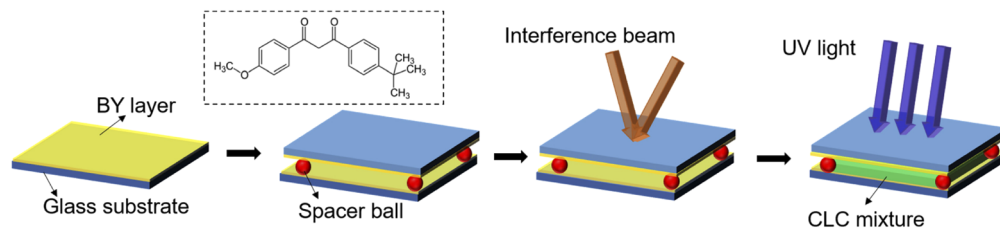

Fig. 4. Fabrication procedures of the proposed broadband CLC lens cell. The inset is the molecular structure of the UV dye.

4. Results and discussion

4.1. Ray-tracing simulation results

The 2D optical layout of the pancake lens is shown in Fig. 5(a). The total track length occupies ~25.6 mm. The modeled structure is composed of a half-mirror, a spherical lens, and a trans-reflective surface with a diffractive or homogeneous pattern. In Fig. 5(b), RGB lines represent the corresponding C, d, F wavelengths, and the green line is set as the primary wavelength. With the increasing FOV, the primary color remains the same, while the other two wavelengths show an apparent color shift. Compared to a traditional system, the lateral color shift of our proposed approach is improved appreciably as shown in Fig. 5(b), especially at a large FOV. The comparisons of standard spot diagrams are shown in Fig. 6. From Fig. 6(a), it is obvious to see that RGB channels are increasingly separated as FOV gets larger. When the CLC lens is laminated to a refractive lens, the spot diagram with RMS radius is improved noticeably as Fig. 6(b) depicts.

4.2. Prototype CAC performance

Before integrating the broadband CLC lens into a pancake VR system, its transmittance spectrum and image quality should be characterized. To properly measure the transmittance of our CLC lens, we used a reference cell to normalize the spectrum. The reference cell is composed of two glass substrates coated with BY and filled with a nematic LC. Firstly, we put the reference cell in a spectrometer with RCP as the incident light to serve as normalized transmittance. Then the
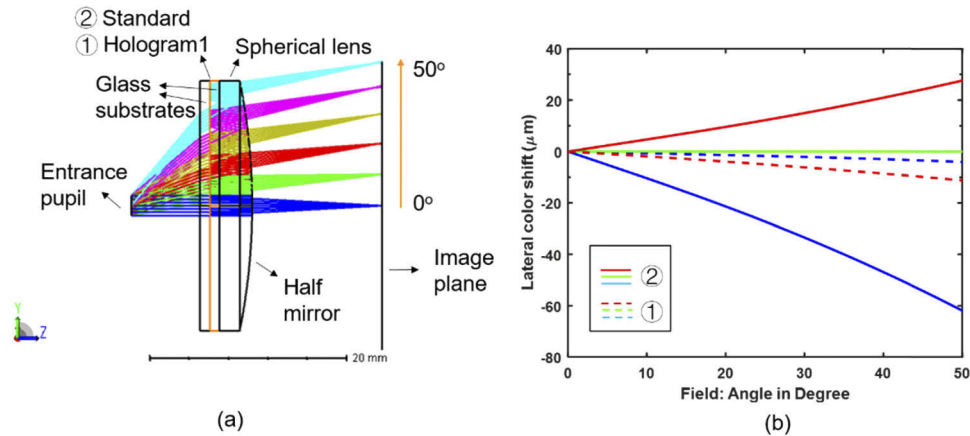
Fig. 5. (a) The 2D optical layout of the modeled device configuration. ① indicates the proposed hybrid pancake lens. ② indicates the traditional pancake lens. (b) Lateral color shift of two cases.
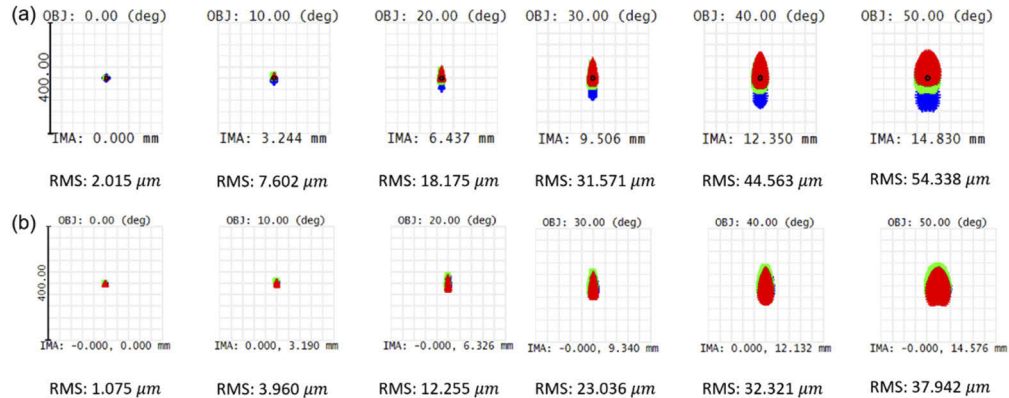

Fig. 6. Standard spot diagrams with RMS radius of (a) a traditional pancake lens and (b) the hybrid pancake lens.

CLC lens was placed in the spectrometer, and we measured its transmittance at normal angle. To make a fair comparison on chromatic aberrations between conventional pancake lens and our hybrid system, we fabricated a CLC cell with a homogeneous pattern to substitute the QWP and the reflective polarizer in the conventional system. Figure 7(a) shows the transmittance spectra of our CLC lens and homogeneous CLC cell. A 1951 USAF resolution target was used to evaluate the image quality. The measurement setup is shown in Fig. 7(b). A diffuser film was combined with a LED flashlight to produce a uniform incident light. Three different colored band-pass filters were incorporated into the system for generating RGB light sources. The central wavelength of the filters is 457 nm, 550 nm, and 633 nm, respectively. The purple circle on the sample indicates the effective lens area. And we used a beam splitter to observe and a camera to capture the images as shown in Figs. 7(c)–7(e). The image quality could be affected by the imperfect alignment of CLC, arising from the patterned alignment and the pitch distribution. The ghost images in the background are caused by the multiple reflections because our substrates and optical elements are without anti-reflection coatings.

The performance of Bragg structure optical elements is sensitive to the incident angle. In practical applications, the incident light has an angular range so that the reflection spectrum
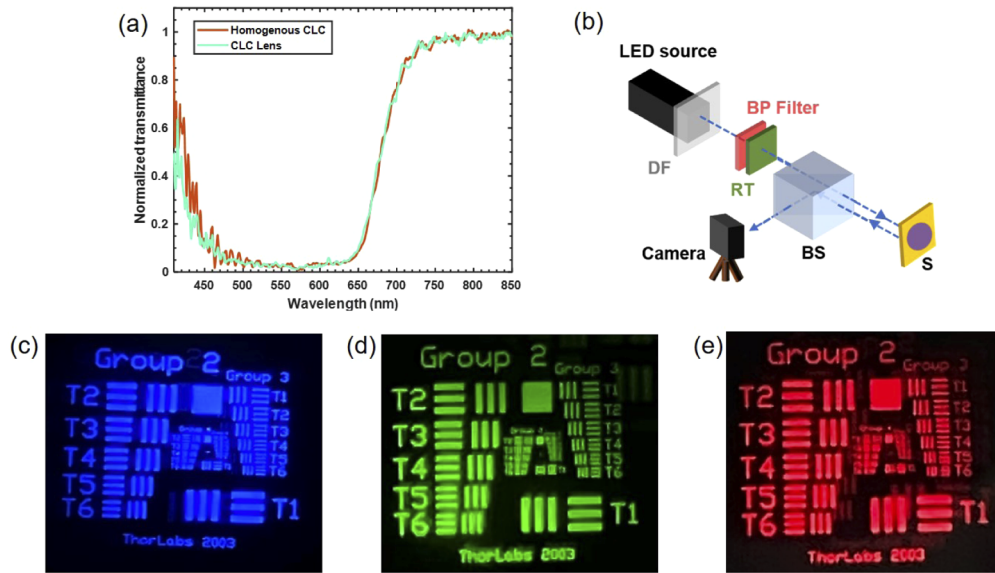
Fig. 7. (a) Measured transmittance spectra of our CLC lens and homogeneous CLC cell. (b) Measurement setup. DF: diffuser film; BP filter: band-pass filter; RT: resolution target; BS: beam splitter; S: sample (broadband CLC lens). (c)-(e) Captured resolution target images of the broadband CLC lens by using band-pass filters at different central wavelengths.

is dependent on the incident angle. Therefore, it is necessary to study the angular-dependent spectral response of the CLC device. Figure 8(a) shows the simulated broadband spectra of the CLC structure with different incident angles. Since the CLC structure has flip symmetry along the optical axis, the spectral response is the same for positive and negative angles. When the incident angle is within ±10°, the spectrum remains almost the same. As the incident angle increases, the reflection band gradually shifts to the blue region. Although the simulation results do not match with the experimental data perfectly, the trend of blue shift is similar, as shown in Fig. 8(b). The mismatch could be caused by the imperfect CLC alignment, including the patterned alignment and the spatial pitch distribution. In our proposed system, the claimed FOV is expressed as the maximum angular size of the object as seen from the entrance pupil, as demonstrated in the 2D layout in Fig. 5(a). Although the system is designed for a large FOV, interestingly, the incident angle on the CLC lens is relatively small. This can be verified by observing the incident rays on the surface of the hologram 1 in Fig. 5(a). Thus, such a small oblique incidence has little influence on the reflection spectra of the CLC lens.

To experimentally verify the CAC performance of the proposed system, we built a miniature pancake lens with 1-inch diameter. An array of letter 'S' in a black background was displayed on a commercial 6.1-inch in-plane switching LCD panel with 1792-by-828 resolution. A broadband right-handed circular polarizer is attached on the LCD panel to produce the desired circular polarization. A 13-nm Ag film was coated on the curved side of the spherical lens to serve as a half-mirror. Due to our limited fabrication facility, the average transmittance and reflection of the Ag film are both 35% across the visible spectrum. That means the trans-reflection efficiency is 12.25%. Our fabricated broadband CLC lens or homogeneous CLC cell was laminated to the flat side of the spherical lens. To suppress light leakage, we inserted a broadband left-handed circular polarizer to block it. Then, an iPhone 11 with an ultrawide-angle lens was used to capture the images. The experimental results are shown in Fig. 9. Figures 9(a) and 9(b) shows the magnified images traveling through the cavity thrice for traditional pancake lens and our
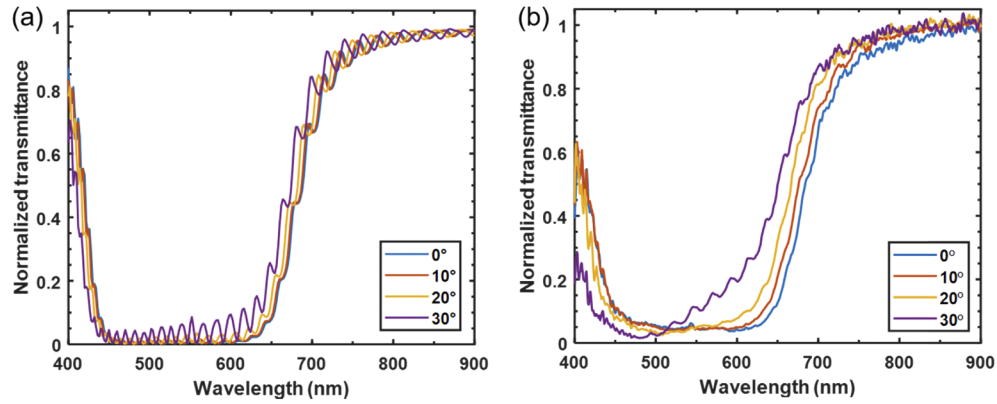
Fig. 8. Angular-dependent normalized transmittance spectra of the CLC devices: (a) simulation results and (b) measured data.

hybrid one, respectively. Both images cover a full FOV of 60°. Recalling our simulation results in Fig. 5(b), the lateral color shift of blue light in two cases is ~5 μm and ~60 μm at 50° viewing angle, respectively, while the lateral color shift of red light is much smaller. By comparing the enlarged parts at the peripheral region between Figs. 9(c) and 9(d), the blue blur at the edges of the letters is diminished by applying the CLC lens. This seems reasonable since the color shift of
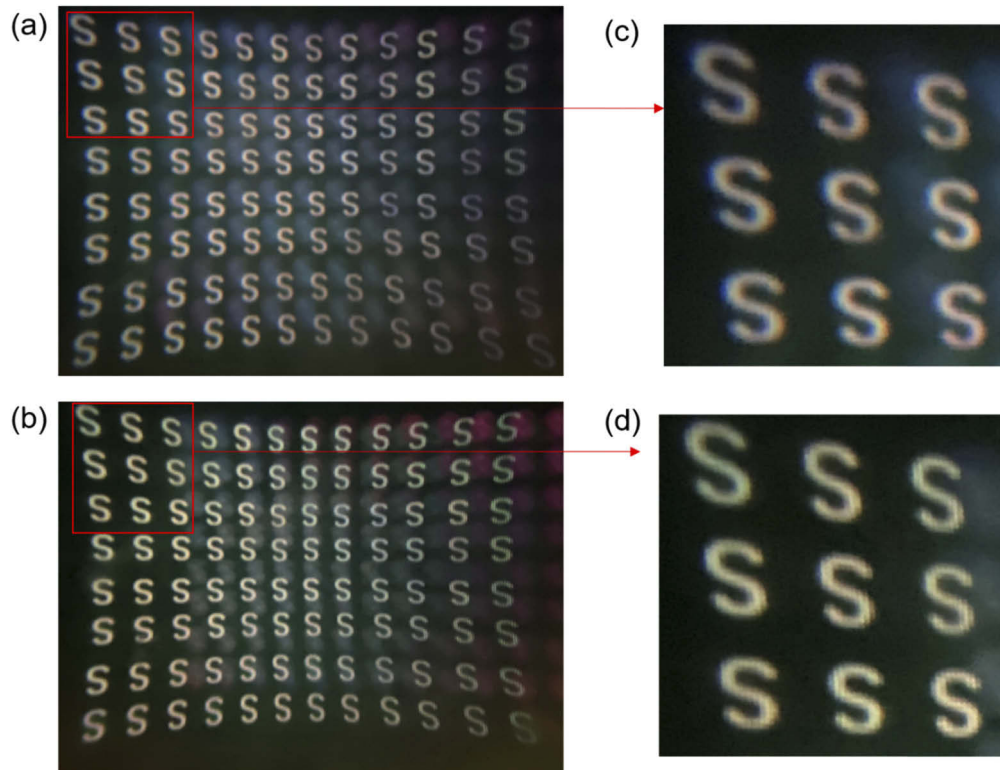

Fig. 9. The captured images through (a) the traditional pancake lens; (b) the proposed hybrid pancake lens. (c) and (d): The zoom-in parts at semi-field 30°.

blue light is easier to distinguish than that of red light. The color variations between the center and corner parts of Figs. 9(a) and 9(b) are caused by the small difference of reflection efficiency over the display spectrum, which can be improved by three methods. 1) To pre-compensate the color variation by slightly tuning the image content. 2) To employ a higher birefringence LC material to further broaden the reflection spectrum and make the efficiency more uniform across the display spectrum. 3) To have a better cell gap control to make the reflection spectra more uniform across the whole area of the cell. The reason for the ghosting is likely twofold. Firstly, the light leakage is caused by the insufficient reflection efficiency of the CLC devices, resulting in a low image contrast. Secondly, there are multiple reflections between the display and glass substrates. Theoretically, the light leakage can be suppressed by utilizing a broadband circular polarizer on the premise that the polarization of light leakage remains unchanged after passing through the CLC lens. However, the imperfect CLC structure may depolarize the leaked light, leading to residual ghosts. The defects in the CLC lens affect the degree of depolarization. Therefore, establishing a good CLC structure is crucial to improve the image contrast. And the multiple reflections can be reduced by coating anti-reflection films on the substrates.

5. Conclusion

In conclusion, we fabricated a broadband CLC lens with 1-inch diameter and 770-mm focal length. The lens manifests decent image quality and high reflection efficiency (>90%) over the display spectrum. Thanks to its polarization-selectivity, the CLC lens can substitute the conventional reflective components, consisting of a QWP and a reflective polarizer, and reduce the chromatic aberration considerably. The proposed polarization-based pancake lens with a weaker chromatic aberration holds promising applications in catadioptric VR viewing optics.

References

1. A. Wexelblat, *Virtual Reality: Applications and Explorations* (Academic, 2014).
2. B. Wheelwright, Y. Sulai, Y. Geng, S. Luanava, S. Choi, W. Gao, and J. Gollier, "Field of view: not just a number," Proc. SPIE **10676**, 1067604 (2018).
3. T. Zhan, K. Yin, J. Xiong, Z. He, and S. T. Wu, "Augmented reality and virtual reality displays: Perspectives and challenges," iScience **23**(8), 101397 (2020).
4. I. Powell, "Lenses for correcting chromatic aberration of the eye," Appl. Opt. **20**(24), 4152–4155 (1981).
5. T. Stone and N. George, "Hybrid diffractive-refractive lenses and achromats," Appl. Opt. **27**(14), 2960–2971 (1988).
6. E. J. Fernández, A. Unterhuber, B. Považay, B. Hermann, P. Artal, and W. Drexler, "Chromatic aberration correction of the human eye for retinal imaging in the near infrared," Opt. Express **14**(13), 6213–6225 (2006).
7. D. E. Roberts, Z. Liao, J. Y. Hwang, S. R. Nersisyan, N. V. Tabirian, D. M. Steeves, B. R. Kimball, and T. J. Bunning, "Chromatic aberration corrected switchable optical systems," Proc. SPIE **10735**, 107350Q (2018).
8. S. W. Nam, S. Moon, B. Lee, D. Kim, S. Lee, C. K. Lee, and B. Lee, "Aberration-corrected full-color holographic augmented reality near-eye display using a Pancharatnam-Berry phase lens," Opt. Express **28**(21), 30836–30850 (2020).
9. S. De Nicola, A. Finizio, G. Pierattini, D. Alfieri, S. Grilli, L. Sansone, and P. Ferraro, "Recovering correct phase information in multiwavelength digital holographic microscopy by compensation for chromatic aberrations," Opt. Lett. **30**(20), 2706–2708 (2005).
10. P. Ferraro, S. Grilli, L. Miccio, D. Alfieri, S. De Nicola, A. Finizio, and B. Javidi, "Full color 3-D imaging by digital holography and removal of chromatic aberrations," J. Disp. Technol. **4**(1), 97–100 (2008).
11. T. Zhan, J. Zou, J. Xiong, X. Liu, H. Chen, J. Yang, S. Liu, Y. Dong, and S. T. Wu, "Practical Chromatic Aberration Correction in Virtual Reality Displays Enabled by Cost-Effective Ultra-Broadband Liquid Crystal Polymer Lenses," Adv. Opt. Mater. **8**(2), 1901360 (2020).
12. J. A. LaRussa and A. T. Gill, "The holographic pancake window TM," Proc. SPIE **0162**, 120–129 (1978).
13. T. L. Wong, Z. Yun, G. Ambur, and J. Etter, "Folded optics with birefringent reflective polarizers," Proc. SPIE **10335**, 103350E (2017).

14. Y. Geng, J. Gollier, B. Wheelwright, F. Peng, Y. Sulai, B. Lewis, N. Chan, W. S. T. Lam, A. Fix, D. Lanman, Y. Fu, A. Sohn, B. Bryars, N. Cardenas, Y. Yoon, and S. McEldowney, "Viewing optics for immersive near-eye displays: pupil swim/size and weight/stray light," Proc. SPIE **10676**, 1067606 (2018).
15. B. A. Narasimhan, "Ultra-Compact pancake optics based on ThinEyes super-resolution technology for virtual reality headsets," Proc. SPIE **10676**, 106761G (2018).
16. J. Kobashi, H. Yoshida, and M. Ozaki, "Planar optics with patterned chiral liquid crystals," Nat. Photonics **10**(6), 389–392 (2016).
17. J. Kim, Y. Li, M. N. Miskiewicz, C. Oh, M. W. Kudenov, and M. J. Escuti, "Fabrication of ideal geometric-phase holograms with arbitrary wavefronts," Optica **2**(11), 958–964 (2015).
18. S. V. Serak, D. E. Roberts, J. Y. Hwang, S. R. Nersisyan, N. V. Tabiryan, T. J. Bunning, D. M. Steeves, and B. R. Kimball, "Diffractive waveplate arrays," J. Opt. Soc. Am. B **34**(5), B56–B65 (2017).
19. T. Zhan, Y. H. Lee, G. Tan, J. Xiong, K. Yin, F. Gou, J. Zou, N. Zhang, D. Zhao, J. Yang, S. Liu, and S. T. Wu, "Pancharatnam–Berry optical elements for head-up and near-eye displays," J. Opt. Soc. Am. B **36**(5), D52–D65 (2019).
20. D. J. Broer, J. Lub, and G. N. Mol, "Wide-Band Reflective Polarizers from Cholesteric Polymer Networks with a Pitch Gradient," Nature **378**(6556), 467–469 (1995).
21. V. T. Tondiglia, L. V. Natarajan, C. A. Bailey, M. M. Duning, R. L. Sutherland, D. K. Yang, A. Voevodin, T. J. White, and T. J. Bunning, "Electrically induced bandwidth broadening in polymer stabilized cholesteric liquid crystals," J. Appl. Phys. **110**(5), 053109 (2011).
22. M. Mitov, "Cholesteric liquid crystals with a broad light reflection band," Adv. Mater. **24**(47), 6260–6276 (2012).
23. Y. Li, T. Zhan, and S. T. Wu, "Flat cholesteric liquid crystal polymeric lens with low f-number," Opt. Express **28**(4), 5875–5882 (2020).
24. W. J. Smith, *Modern lens design* (McGraw-Hill, 2005).
25. W. T. Welford, *Aberrations of Optical Systems* (CRC, 1986).